

Distance to Galactic globulars using the near-infrared magnitudes of RR Lyrae stars: IV. The case of M5 (NGC 5904)

G. Coppola^{1*}, M. Dall’Ora¹, V. Ripepi¹, M. Marconi¹, I. Musella¹, G. Bono^{2,3,4}, A. M. Piersimoni⁵, P. B. Stetson⁶ and J. Storm⁷

¹ *INAF–OACN, Via Moiariello 16, 80131, Napoli, Italy*

² *Dipartimento di Fisica– Univ. di Roma Tor Vergata, via della Ricerca Scientifica 1, 00133 Roma, Italy*

³ *INAF–Osservatorio Astronomico di Roma, Via Frascati 33, 00040, Monte Porzio Catone, Italy*

⁴ *European Southern Observatory, Karl-Schwarzschild-Str. 2, 85748 Garching bei Munchen, Germany*

⁵ *INAF–OACTe, via M. Maggini, 64100 Teramo, Italy*

⁶ *DAOHIA, NRC, 5071 West Saanich Road, Victoria, BC V9E 2E7, Canada*

⁷ *AIP, An der Sternwarte 16, D-14482 Potsdam, Germany*

Accepted: Received:

ABSTRACT

We present new and accurate near-infrared (NIR) J , K -band time series data for the Galactic globular cluster (GC) M5 = NGC 5904. Data were collected with SOFI at the NTT (71 J + 120 K images) and with NICS at the TNG (25 J + 22 K images) and cover two orthogonal strips across the center of the cluster of $\approx 5 \times 10$ arcmin² each. These data allowed us to derive accurate mean K -band magnitudes for 52 fundamental (RR_{ab}) and 24 first overtone (RR_c) RR Lyrae stars. Using this sample of RR Lyrae stars, we find that the slope of the K -band Period Luminosity (PLK) relation (-2.33 ± 0.08) agrees quite well with similar estimates available in the literature. We also find, using both theoretical and empirical calibrations of the PLK relation, a true distance to M5 of 14.44 ± 0.02 mag. This distance modulus agrees very well (1σ) with distances based on main sequence fitting method and on kinematic method (14.44 ± 0.41 mag, Rees 1996), while is systematically smaller than the distance based on the white dwarf cooling sequence (14.67 ± 0.18 mag, Layden et al. 2005), even if with a difference slightly larger than 1σ . The true distance modulus to M5 based on the PLJ relation (14.50 ± 0.08 mag) is in quite good agreement with the distance based on the PLK relation further supporting the use of NIR PL relations for RR Lyrae stars to improve the precision of the GC distance scale.

Key words: Stars:distances - Stars:horizontal branch - Galaxy:globular clusters:individual:M5

1 INTRODUCTION

Galactic Globular Clusters (GGCs) are crucial stellar systems to constrain the input physics adopted to construct evolutionary and pulsation models (Renzini & Fusi Pecci 1988; Marconi et al. 2003; Cassisi 2010), to investigate the kinematic properties of gas-poor, compact systems (Meylan & Heggie 1997) and to constrain the formation and evolution of the Galactic spheroid (halo, thick disk, bulge; e.g. Mackey & van den Bergh 2005; Bica et al. 2006; Forbes & Bridges 2010). The GGCs often host RR Lyrae

variables (RRLs), which are fundamental distance indicators for low-mass, old stellar populations. They are bright enough to have been detected in several Local Group galaxies (e.g. Dall’Ora et al. 2003, 2006; Pietrzyński et al. 2008; Greco et al. 2009; Fiorentino et al. 2010; Yang et al. 2010). They can also be easily identified, since they have characteristic light curves and periods. The most popular methods to estimate their distances are the visual magnitude – metallicity relation and the near-infrared (NIR) Period-Luminosity (PL) relation (e.g. Bono 2003; Cacciari & Clementini 2003). The reader interested in other independent approaches based on RRL to estimate stellar distances is referred to

* E-mail: coppola@na.astro.it

the thorough investigations by, e.g., Marconi et al. (2003); Di Criscienzo et al. (2004); Feast et al. (2008).

The visual magnitude – metallicity approach appears to be hampered by several theoretical and empirical uncertainties affecting both the zero-point and the slope (Bono et al. 2003). The NIR PL relation seems very promising, since it shows several indisputable advantages. Dating back to the seminal investigation by Longmore et al. (1986) it has been demonstrated on empirical basis that RRL do obey to a well defined K -band PL relation. The key reason why the PL relation shows up in the NIR bands is mainly due to the fact that the bolometric correction in the NIR bands, in contrast with optical bands, steadily decreases when moving from hotter to cooler RRLs. This means that they become brighter as they get cooler. The pulsation periods –at fixed stellar mass and luminosity– become longer, since cooler RRLs have larger radii. The consequence is a stronger correlation between period and magnitude when moving from the I - to the K -band.

The advantages of using NIR PL relations to estimate distances are manifold.

i) Evolutionary and pulsation predictions indicate that the NIR PL relations are minimally affected by evolutionary effects inside the RRL instability strip. The same outcome applies for the typical spread in mass inside the RRL instability strip (Bono et al. 2001, 2003). This means that individual RRL distances based on the NIR PL relations are minimally affected by systematics introduced by their intrinsic parameters and evolutionary status. *ii)* Theory and observations indicate that fundamental (F or RR_{ab}) and first overtone (FO or RR_c) RRL do obey independent NIR PL relations that are linear over the entire period range covered by F and FO pulsators.

The NIR PL relations together with the aforementioned features have also three positive observational advantages.

a) The NIR magnitudes are minimally affected by reddening uncertainties. This means that the RR Lyrae NIR PL relations can provide robust distance estimates for systems affected by differential reddening. *b)* The luminosity amplitude in the NIR bands is at least a factor of 2-3 smaller than in the optical bands. Therefore, accurate estimates of the mean NIR magnitudes can be obtained with a modest number of observations. Moreover, empirical light curve templates (Jones et al. 1996) can be adopted to improve the accuracy of the mean magnitude even when only a single observation is available. *c)* Thanks to the unprecedented effort by the 2MASS project (Skrutskie et al. 2006), accurate samples of local NIR standard stars are available across the sky. This means that both relative and absolute NIR photometric calibrations do not require supplementary telescope time.

The use of the NIR PL relations is also affected by four drawbacks.

– Empirical estimates of the slope of NIR PL relations show a significant scatter from cluster to cluster. They range from ~ -1.7 (IC4499 Sollima et al. 2006) to ~ -2.9 (M55, Sollima et al. 2006) and it is not clear yet whether this change is either intrinsic or caused by possible observational biases. – Both theoretical and empirical investigations of the PLK show a not-negligible scatter of the zero point. This is a crucial point, as we plan to adopt the PLK as a tool to derive distances. Indeed, if we set as a reference

$\log P = -0.5$ and $[Fe/H] = -1.5$, the most robust absolute magnitude estimates range from $M_{K,-0.5,-1.5} = -0.33$ (infrared flux method, Longmore et al. 1990) to $M_{K,-0.5,-1.5} = -0.46$ (HB models, Catelan et al. 2004; empirical calibration Sollima et al. 2006), with intermediate values of $M_{K,-0.5,-1.5} = -0.39$ (pulsational models Bono et al. 2001; HB models, Cassisi et al. 2004).

– Evolutionary and pulsation predictions indicate that the intrinsic spread of the NIR PL relations decreases as soon as either the metallicity or the HB-type of the Horizontal Branch (HB) is taken into account (Bono et al. 2003; Cassisi et al. 2004; Catelan et al. 2004; Del Principe et al. 2006). This means that accurate distance estimates of field RRLs do require an estimate of the metallicity. Moreover, no general consensus has been reached yet concerning the value of the coefficient of the metallicity term in the NIR Period-Luminosity-Metallicity (PLZ) relations. The current estimates for the K -band range from 0.08 (Sollima et al. 2006) to 0.23 (Bono et al. 2003) mag/dex based on cluster and field RRLs, respectively.

– The use of the template light curves does require for each object accurate estimates of B/V-band amplitudes and of the epoch of maximum.

To address these problems our group undertook a long-term project aimed at providing homogeneous and accurate NIR photometry for several GCs hosting sizable samples of RRLs and covering a wide range of metallicities. We have already investigated the old LMC cluster Reticulum (Dall’Ora et al. 2004, hereinafter paper I), the GGC M92 (Del Principe et al. 2005, hereinafter paper II) and ω Centauri (Del Principe et al. 2006, hereinafter paper III).

In this paper we present new results for the GGC M5 (NGC5904). This system is a typical *halo* globular cluster, and indeed, it is located at a distance of only ~ 7 kpc from the Sun, 5.5 kpc from the Galactic Center, and 4.9 kpc above the Galactic disc (Zinn 1985); its space motion is ~ 490 km s⁻¹ (Cudworth & Hanson 1993). Moreover, it has a low reddening ($E(B - V) = 0.03$, according to the Harris catalog, Harris 1996, and its new revision Harris 2010) and metal-intermediate composition, with estimates ranging from -1.0 dex (Butler 1975) to -1.346 dex (Carretta et al. 2009). This cluster is a very good target to investigate the NIR PLZ relation, since it hosts a rich sample of RRLs (~ 130 in the 2002 release of the Clement’s on-line catalog, Clement et al. 2001). The RR_{ab} stars have an average period of ~ 0.55 d, making M5 as one of the classical Oosterhoff type I clusters (Oosterhoff 1939). It is located only two degrees from the celestial equator, and therefore, the search for cluster variables has been performed using telescopes from both hemispheres. According to Sawyer Hogg (1973) a total of 97 variables were present in M5 and among them 93 were RRLs. A significant fraction of these variables were discovered by Bailey & Pickering (1917) with the remaining stars identified by Oosterhoff (1941). The central regions of M5 have been surveyed photographically by Gerashchenko (1987) and Kravtsov (1988) who found an additional 27 variables. Subsequently, Cohen & Matthews (1992) supplemented the catalog with five other variables, while Reid (1996) presented observations of 49 RRLs, three of which were new discoveries. Brocato et al. (1996) added 15 new variables located across the central regions of the cluster. More recent investigations

by Sandquist et al. (1996) and Drissen & Shara (1998) identified 28 previously unknown variables, while Kaluzny et al. (2000) and Caputo et al. (1999) identified 32 new variables. We end up with a sample of 102 variable stars, and among them 71 are F and 31 FO RRLs.

The paper is organized as follows: in Sec. 2 we discuss the observations and the strategy adopted to perform the photometry and to calibrate the data. The RRL properties and the approach adopted to determine their light curves are presented in Sec. 4, while in Sec. 5 we present the PLK and the PLJ relations. Finally, in Sec. 6, we summarize the current findings and briefly outline future perspectives.

2 OBSERVATIONS AND DATA REDUCTION

We collected J and K_s images in six different runs from February 2001 to March 2002 with SOFI@NTT/ESO¹ and J and K' data in two runs in May 2005 and July 2005 with NICS@TNG². The SOFI data were collected in the large field mode with a pixel scale of 0.292 arcsec/pixels and with a field of view of $4'.94 \times 4'.94$. NICS was also used in the large field mode, with pixel scale of 0.25 arcsec/pixels and with a field of view of $4'.2 \times 4'.2$. For both instruments, observations were obtained of off-target fields for the sky subtraction. Since the cluster is moderately extended (tidal radius ~ 28.4 arcmin, Harris 2010), for both instruments two different pointings were observed, mapping the cluster in the North-South direction (SOFI) and in the East-West direction (NICS), covering two strips of about 5×5 arcmin² in both directions (see Fig. 1). We collected 71 (228 s of total exposure) J - and 120 (1529 s) K_s -bands useful frames with SOFI, and 25 (193 s) J - and 22 (184 s) K' -bands images with NICS. The number of epochs for recovered RRLs ranges from 1 to 16. The log of observations is given in Table 1.

The raw SOFI frames were first corrected for the cross-talk effect with the IRAF³ procedure `crosstalk.c1`, available in the SOFI web pages. Data were then pre-processed with our IRAF-based custom pipeline, which corrects for bias, flat field and bad pixel mask, and subtracts the sky contribution with a two-step technique as described in Pietrzyński & Gieren (2002). The NICS images were corrected for cross-talk with a FORTRAN program made available in the NICS web pages, and thereafter pre-processed with the same pipeline described above, without applying any bad pixel mask.

2.1 Photometry

For each image, a preliminary PSF model and a list of stars were produced with the DAOPHOTIV/ALLSTAR package (Stetson 1987, 1994). In order to cross-match individual star catalogs, we computed geometric transformations with the DAOMATCH/DAOMASTER programs (Stetson 1994),

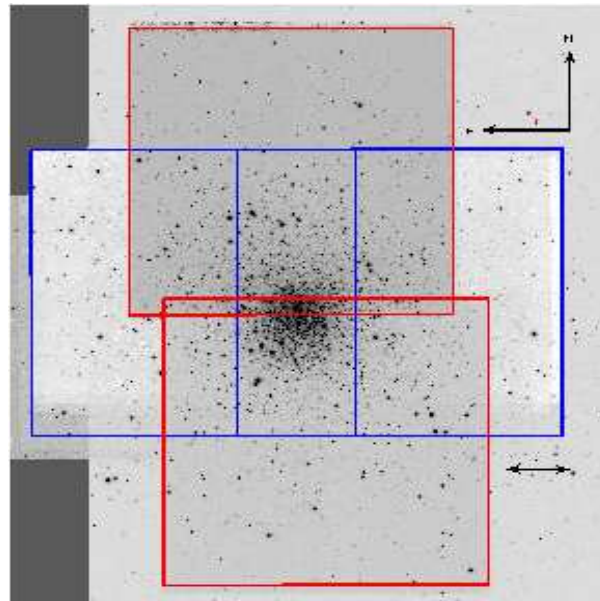


Figure 1. The coverage of the two data sets collected with the SOFI@NTT/ESO telescope (red squares) and NICS@TNG (blue squares), superimposed to M5. The showed picture has been obtained by aligning the NIR images to a WFI@2.2 MPG/ESO I -band reference frame

using as a reference a 2.2@MPG/ESO I -band image, available in the ESO data archive. A master star list was therefore produced on the total stacked image. We then performed a first ALLFRAME (Stetson 1994) run, and a second star list was built on the median of the star-subtracted input images, which was merged with the previous one, in order to get a more complete input catalog. New accurate, spatially varying, PSF models were subsequently computed on the individual images, after cleaning each PSF star of contamination by faint neighbors, and a second ALLFRAME run was performed. We ended up with a final catalog of 38,131 sources.

2.2 Calibration

We calibrated each individual image to the Two Micron All Sky Survey (2MASS) photometric system, by selecting clean local 2MASS standards (i.e. bright and reasonably isolated, by taking advantage of the 2MASS photometric flags). The SOFI images collected before April 2003 are affected, due to the misalignment of the Large Field objective, by a strong distortion on a strip of ~ 200 pixels wide along the x -axis. We found that the difference between instrumental and 2MASS magnitudes can attain values of the ~ 0.3 magnitudes in this region of the detector. Therefore, we wrote an ESO-MIDAS (Munich Image Data Analysis System) procedure to simultaneously correct for this positional effect and to get standard photometric zero-points. The procedure performs a polynomial regression of the instrumental magnitude as a function of the x , y and 2MASS magnitude variables. The accuracy of the calibration, evaluated as the standard deviation of the fit, varies with the images from approximately 0.01 to 0.06 mag. We explicitly note that a spatially varying PSF might introduce a positional effect. How-

¹ <http://www.eso.org/sci/facilities/lasilla/instruments/sofi/overview.html>

² <http://www.tng.iac.es/instruments/nics/>

³ IRAF is distributed by the National Optical Astronomical Observatory, which is operated by the Association of Universities for Research in Astronomy, Inc., under cooperative agreement with the National Science Foundation.

Table 1. Observing Log. The first column shows the date of observation, written as day/month/year. The second, third, fourth and fifth column list the instrument used, the filter, the number of epochs collected and the total exposure time, respectively. The last column reports the average seeing, computed as the median seeing measured on the individual images.

DATE	INSTRUMENT	FILTER	EPOCHS	TOTAL EXP. TIME (sec)	<SEEING> (arcsec) (arcsec)
050201	SOFI	<i>J</i>	2	18	0.71
		<i>K_s</i>	2	120	0.74
070201	SOFI	<i>J</i>	2	18	0.74
		<i>K_s</i>	2	108	0.63
240202	SOFI	<i>J</i>	4	36	0.96
		<i>K_s</i>	4	228	0.75
250202	SOFI	<i>J</i>	6	54	0.66
		<i>K_s</i>	6	348	0.58
260202	SOFI	<i>J</i>	5	45	0.92
		<i>K_s</i>	5	300	0.93
090302	SOFI	<i>J</i>	6	57	0.72
		<i>K_s</i>	6	425	0.71
130505	NICS	<i>J</i>	2	105	0.50
		<i>K'</i>	2	80	0.45
180705	NICS	<i>J</i>	2	88	0.66
		<i>K'</i>	2	104	0.65

ever, to overcome this problem the selected PSF stars for each image are uniformly distributed across the frame. The difference between instrumental and 2MASS magnitudes in the region not affected by distortions is minimal. Therefore the positional effect seems to be caused by the objective misalignment.

We did not include color terms in the calibration, since they are negligible in the range of colors of interest. The SOFI data have minimal color dependence, as shown in the SOFI web pages⁴, while the NICS *K'*-band data typically have a non-negligible dependence on the color, which in the original transformation by Wainscoat & Cowie 1992 is given in terms of the *H* – *K* color. In fact, by combining the transformation between the *K'* and the standard *K* filter in the Caltech photometric system (CIT, Frogel et al. 1978), as described in Wainscoat & Cowie (1992), with the transformations between the 2MASS and the CIT systems (Carpenter 2001), we end up with the following transformation: $K_{2M} = K' - 0.2 \times (H - K)_{CIT}$. Since the typical (*H* – *K*) HB colors range from –0.1 to +0.05, and considering that the RRL Instability Strip is confined to an even narrower color range, we conclude that the maximum systematic error is ~ 0.01 magnitudes.

3 THE COLOR-MAGNITUDE DIAGRAM

Fig. 2 shows the observed *K*–(*J* – *K*) color-magnitude diagram. Stars plotted in this figure were selected by choosing only stars with small photometric contamination by close companions, using the SEPARATION index (Stetson et al. 2003). The contamination limit was set to 3, meaning that we selected only stars whose ratio (expressed in magnitudes) between the central surface brightness and the sum of the

brightnesses of all other stars out to $10\times$ the FWHM is equal or larger than 3 (= a factor of 16 in flux). This means that we selected only stars whose correction for photometric contamination by other stars was smaller than $\sim 15\%$. Since ALLFRAME fits the PSF model on each individual star when all the other stars in the image have been digitally subtracted, any uncorrected photometric contamination remaining should therefore be much smaller. We show only stars with estimated ALLFRAME photometric standard errors smaller than 0.04 mag, both in the *J* and *K* band, corresponding to a signal-to-noise ratio on individual images of $S/N \sim 5$. Below this limit, we consider that the measurements on the individual images do not have sufficient accuracy to be included in our catalog. Adopting these cuts, we end up with 11800 star-like sources. Red and green filled circles represent RR_{ab} and RR_c stars (see below), while cyan filled circles show variable stars excluded from the PLK and PLJ analysis (see Sec. 5). Our photometry covers the full range of magnitudes running from the Tip of the Red Giant Branch (RGB, *K* ~ 8) down to ≈ 0.5 magnitude below the Turn-Off (TO, *K* ~ 17) region. The photometric limit can therefore be approximately located at *K* ≈ 18 mag, where the intrinsic photometric uncertainty is of the order of ~ 0.03 mag in the *K* band. The CMD clearly shows the bump of the RGB, at *K* ≈ 13 mag, as well as the separation between the RGB and the Asymptotic Giant Branch (*K* ≈ 12.5). The intrinsic features of the CMD and a comparison with evolutionary predictions will be addressed in a forthcoming paper.

4 RR LYRAE STARS

We recovered 102 out of 131 RR Lyrae variables on the basis of the WCS positions listed in the catalogs by Evstigneeva et al. (1999) and Samus et al. (2010). The 29 RRLs not included in the current sample are located outside the region covered by our data. Barycentric Julian days were

⁴ http://www.eso.org/sci/facilities/lasilla/instruments/sofi/inst/setup/Zero_Point.html

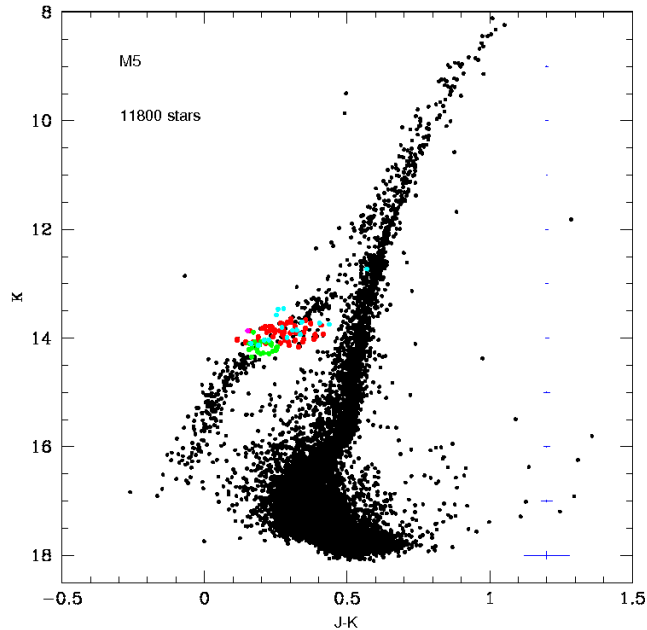


Figure 2. K , $(J-K)$ Color-Magnitude Diagrams of the globular M5. Red and green circles mark the position of RR_{ab} and RR_c variables, respectively. The cyan filled circles show variables neglected in the estimate of the distance. The error bars on the right display intrinsic errors in magnitude and in color. The number of selected stars is also labeled.

computed for each epoch of observation. The total exposure for each epoch was split into a number of shorter frames, and the final mean magnitude was estimated as an average of the measurements over all the individual frames. The K -band light curves of RRLs are almost sinusoidal and the luminosity amplitude in this band is also modest. However, the most accurate results for the mean magnitudes are achieved by using the light curve templates provided by Jones et al. (1996). The use of the template yields accurate mean magnitudes even when only a single epoch is available. Note that the use of the template requires accurate ephemerides and B -band amplitudes. Therefore, we mined the available literature to get updated periods, epochs of maxima and B -band amplitudes. In most cases the B -band amplitude was not available, and we transformed the V -band amplitude into the B -band one using the relation $A_B = 1.264 * A_V + 0.028$ (Jones et al. 1996). Table 2 lists our adopted parameters: the name of the variable (following the number scheme proposed in Caputo et al. 1999), the adopted period with the related reference, the epoch of maximum with the associated reference, the computed intensity-averaged K -band magnitude with the uncertainty σ , the variable type (fundamental, first overtone or Blazkho RRLs) and the B -band amplitude A_B , with the reference. For the Blazkho RRLs we follow the classification proposed by Jurcsik et al. (2010). Moreover, in several cases the period and the epoch of maximum were not available from the same reference, and we imposed a shift to the phased light curve to reasonably match the template. Shifts are listed in column 8 of Table 2. Finally, column 9 lists the adopted V -band magnitude as extracted by the optical light curves of the unpublished archive of author PBS. In some cases the epoch was not available in literature and we used the epoch of our first measure to calculate

the intensity-averaged K -band magnitude. It is worth noting that period changes among the M5 RRLs have been detected by Storm et al. (1991); Reid (1996); Szeidl et al. (2010), but these changes are minimal and do not affect the conclusions of this investigation. An updated and homogeneous photometric catalog of the M5 RRLs is highly desirable. Note that RRLs for which the B/V amplitude was not available in the literature were neglected. The intensity-weighted mean magnitudes –computed by DAOMASTER– of these objects are listed in column 4 of Table 2. We also excluded a few variables that were heavily contaminated by bright neighbors or by close companions (see Sec. 4.1). The distance estimates based on the PLK relation rely on 52 RR_{ab} and 24 RR_c variables. Some example of RRL light curves are depicted in Fig. 3. Black and red filled circles represent the SOFI and the NICS observations, respectively. The complete atlas of the light curves is available in the electronic version of this paper.

4.1 Notes on individual variables

V25: for this variable we did not find any amplitude information in the literature. However since the pulsation cycle was evenly covered, we fitted the observed data with a spline curve, getting a light curve (red curve in Fig. 3) with a shape very similar to the template available for similar periods.

V84: actually this variable is a type II Cepheid, whose K -band light curve was presented by Matsunaga et al. (2006), and it is included in our photometric catalog. Unfortunately, most of our measurements of this star are above the non-linearity level, and we were not able to produce a reliable light curve.

V86: this variable is heavily contaminated by close neigh-

Table 2. Summary of the light curve parameters and properties of the M5 RRLs. *Col. 1:* identification star; *Col. 2:* adopted period with reference; *Col. 3:* adopted epoch with reference; *Col. 4:* derived intensity-averaged *K*-band magnitude; *Col. 5:* derived uncertainty on intensity-averaged *K*-band magnitude; *Col. 6:* type; *Col. 7:* adopted *B*-band amplitude with reference; *Col. 8:* adopted shift of the phase; *Col. 9:* adopted *V*-band magnitude as extracted by light curves of the private archive of author PBS.

Var	Period (Ref.) [d]	Epoch (Ref.) (JD)	$\langle K \rangle$ mag	σ mag	Type	A_B (Ref.)	$\Delta\phi$	(V)	Note
V1	0.5217868 (S10)	48399.795 (R96)	13.981	0.003	BI	1.43 (K00)	-0.05	15.238	no PLJ
V4	0.449699 (K00)	48399.732 (R96)	14.169	0.003	BI	1.24 (K00)	-0.40	15.043	
V5	0.54584 (R96)	48399.787 (R96)	13.920	0.003	BI	1.42 (R96)	-0.05	15.188	no PLJ
V6	0.54882 (R96)	48399.743 (R96)	13.853	0.002	RR _{ab}	1.18 (R96)	-0.30	15.225	
V7	0.494404 (S91)	46931.867 (S91)	14.031	0.003	RR _{ab}	1.58 (S91)	+0.10	14.959	no PLJ
V11	0.595911 (K00)	48399.800 (R96)	13.714	0.009	RR _{ab}	1.43 (K00)	+0.12	14.949	no PLJ
V12	0.46770 (R96)	48399.827 (R96)	14.064	0.008	RR _{ab}	1.53 (R96)		15.066	no PLJ
V13	0.51313 (R96)	48424.744 (R96)	13.848	0.003	RR _{ab}	1.40 (R96)	-0.40	14.861	
V14	0.48733 (R96)	48399.764 (R96)	14.036	0.004	BI	1.64 (R96)	-0.05	15.119	
V16	0.647634 (K00)	48400.734 (R96)	13.730	0.003	RR _{ab}	1.53 (K00)		14.887	no PLJ
V17	0.601395 (S10)	52331.772*	13.793	0.003	RR _{ab}	1.44 (S10)	-0.20	14.912	
V18	0.464 (S91)	46931.722 (S91)	13.984	0.010	BI	1.58 (K00)		15.221	no PLJ
V24	0.48125 (R96)	48400.702 (R96)	14.139	0.003	BI	0.96 (R96)	-0.10	14.983	no PLJ
V25	0.5074854 (S10)	51947.026*	13.940		RR _{ab}			15.133	
V26	0.623978 (S10)	52331.892*	13.71**		RR _{ab}			14.973	no PLK/PLJ
V27	0.47034 (R96)	48404.890 (R96)	14.074	0.002	BI	1.44 (R96)		14.994	
V28	0.543926 (S91)	48400.710 (R96)	13.925	0.012	RR _{ab}	1.25 (K00)		15.075	no PLJ
V30	0.592207 (K00)	46931.320 (S91)	13.893	0.003	BI	1.07 (K00)	-0.05	15.082	no PLJ
V33	0.501575 (K00)	48812.701 (R96)	14.064	0.003	RR _{ab}	1.51 (K00)		14.917	
V34	0.568119 (K00)	48399.838 (R96)	13.932	0.003	RR _{ab}	1.04 (K00)	+0.30	15.086	no PLJ
V35	0.3081343 (S10)	48400.745 (R96)	14.131	0.003	RR _c	0.61 (K00)		15.009	
V36	0.626980 (R96)	48400.818 (R96)	13.746	0.003	RR _{ab}	0.81 (R96)	+0.20	15.041	
V37	0.4887954 (S10)	51946.869*	13.94**		RR _{ab}			15.049	no PLK/PLJ
V38	0.4704285 (S10)	48399.762 (R96)	14.021	0.003	RR _{ab}	1.24 (R96)	+0.10	15.038	
V39	0.589035 (K00)	51946.751*	13.845	0.003	RR _{ab}	1.51 (K00)		15.116	
V40	0.317334 (K00)	48424.744 (R96)	14.157	0.003	RR _c	0.57 (K00)		15.067	
V41	0.488577 (K00)	52331.697*	13.995	0.003	RR _{ab}	1.37 (K00)		15.239	
V43	0.66023 (R96)	48424.762 (R96)	13.648	0.026	RR _{ab}	0.89 (R96)		15.093	no PLJ
V44	0.329576 (K00)	48401.865 (R96)	14.043	0.003	RR _c	0.56 (K00)		14.959	
V45	0.616595 (B96)	48400.888 (R96)	13.627	0.002	RR _{ab}	1.78 (B96)		15.035	
V47	0.539739 (K00)	48404.910 (R96)	13.939	0.003	RR _{ab}	1.34 (K00)		15.121	
V52	0.501785 (K00)	48424.740 (R96)	13.046	0.003	BI	0.74 (R96)		14.997	
V53	0.373594 (B96)	51946.832*	13.889	0.003	RR _c	0.54 (B96)		14.773	
V54	0.454239 (K00)	48399.732 (R96)	14.099	0.003	RR _{ab}	1.53 (K00)	+0.25	15.272	
V55	0.3289023 (S91)	46931.498 (S91)	14.113	0.003	RR _c	0.55 (S10)		15.101	
V56	0.53468 (R96)	48424.771 (R96)	13.894	0.002	BI	0.96 (R96)	-0.06	15.217	
V57	0.284673 (K00)	48399.770 (R96)	14.289	0.003	RR _c	0.65 (K00)		14.995	
V59	0.542027 (K00)	48399.740 (R96)	13.908	0.004	RR _{ab}	1.28 (K00)	0.15	15.031	
V60	0.285274 (O99)	51946.726*	14.281	0.003	RR _c	0.71 (S10)		15.027	
V64	0.544492 (K00)	51946.923*	14.050	0.003	RR _{ab}	1.32 (K00)		15.057	
V65	0.480758 (K00)	48404.897 (R96)	14.074	0.003	BI	0.99 (R96)	-0.25	15.317	no PLJ
V77	0.8451232 (K00)	51946.954*	13.450	0.011	RR _{ab}	0.79 (K00)		14.706	no PLJ
V78	0.264798 (K00)	48399.865 (R96)	14.350	0.003	RR _c	0.52 (K00)		15.098	
V79	0.333089 (K00)	48400.725 (R96)	14.070	0.003	RR _c	0.47 (K00)		15.071	
V80	0.336549 (K00)	48400.702 (R96)	14.073	0.003	RR _c	0.52 (K00)		15.064	
V81	0.55731406 (B96)	48399.764 (R96)	13.893	0.002	RR _{ab}	1.21 (B96)	-0.30	15.080	no PLJ
V82	0.558927 (K00)	48399.791 (R96)	13.866	0.003	RR _{ab}	1.19 (K00)		15.055	
V83	0.553329 (R96)	48399.805 (R96)	13.862	0.002	RR _{ab}	1.09 (R96)	+0.25	15.085	
V85	0.5275226 (S10)	51946.869*	13.75**		RR _{ab}			14.861	no PLK/PLJ
V86	0.56728 (B96)	51947.124*	13.717	0.003	RR _{ab}	1.57 (B96)		14.731	no PLK/PLJ-crowded
V87	0.7383982 (S10)	48400.841 (R96)	13.651	0.003	RR _{ab}	0.49 (S10)		14.922	
V88	0.328070 (K00)	48404.910 (R96)	14.092	0.003	RR _c	0.57 (K00)	+0.25	14.940	
V89	0.558454 (K00)	48400.793 (R96)	13.852	0.003	RR _{ab}	1.22 (K00)	+0.05	15.169	
V90	0.5571570 (S10)	51946.757*	13.86**		RR _{ab}			15.060	no PLK/PLJ

Table 2 – continued

Var	Period (Ref.) [d]	Epoch (Ref.) (JD)	$\langle K \rangle$ mag	σ mag	Type	A_B (Ref.)	$\Delta\phi$	(V)	Note
V91	0.60139 (R96)	48401.834 (R96)	13.787	0.003	RR _{ab}	1.44 (R96)	-0.05	15.125	
V92	0.4633870 (S10)	51946.684*	13.99**		RR _{ab}			15.199	no PLK/PLJ
V93	0.552875 (O99)	51946.814*	13.73**		RR _{ab}			14.967	no PLK/PLJ
V94	0.51225 (R96)	48424.788 (R96)	13.971	0.003	RR _{ab}	1.22 (R96)		15.107	no PLJ
V95	0.2907655 (S10)	52331.021*	14.222	0.003	RR _c	0.66 (S10)		15.037	
V96	0.46424 (R96)	48399.806 (R96)	13.915	0.003	RR _{ab}	0.86 (R96)	+0.40	15.079	no PLK/PLJ-crowded
V97	0.54469 (R96)	48399.850 (R96)	13.891	0.002	Bl	0.67 (R96)		15.000	no PLJ
V98	0.30641 (B96)	51946.870*	14.190	0.003	RR _c	0.68 (S10)		14.958	no PLJ
V99	0.321340 (R96)	48401.921 (R96)	14.120	0.003	RR _c	0.61 (R96)		14.907	
V100	0.294360 (R96)	48399.761 (R96)	14.224	0.004	RR _c	0.72 (R96)		15.061	
V103	0.5667 (C99)	47629.551 (C99)	13.771	0.003	RR _{ab}	1.03 (C99)	-0.36	15.019	
V104	0.310930 (O99)	52331.862*	14.044	0.003	RR _c	0.9 (C99)		15.048	no PLK/PLJ
V105	0.2920 (C99)	47629.813 (C99)	14.107	0.007	RR _c	0.94 (C99)		14.882	
V106	0.5624 (C99)	47629.311 (C99)	13.652	0.007	RR _{ab}	1.20 (C99)	0.05	14.804	no PLK/PLJ-crowded
V107	0.5117 (C99)	47629.776 (C99)	13.703	0.005	RR _{ab}	1.52 (C99)		14.767	no PLK/PLJ-crowded
V108	0.329 (C99)	51946.902*	13.913	0.004	RR _c	0.55 (C99)		14.802	no PLK/PLJ-blended?
V109	0.476 (C99)	47629.854 (C99)	14.069	0.003	RR _{ab}	1.55 (C99)		15.127	no PLJ
V110	0.598528 (O99)	51946.779*	13.838	0.003	RR _{ab}	0.95 (C99)		15.218	
V111	0.6233 (C99)	47629.283 (C99)	13.456	0.009	RR _{ab}	0.93 (C99)		15.018	no PLK/PLJ-crowded
V112	0.5367 (C99)	47629.546 (C99)	13.858	0.003	RR _{ab}	1.29 (C99)		14.941	
V113	0.2843 (C99)	47629.758 (C99)	14.185	0.003	RR _c	0.70 (C99)		14.913	
V114	0.604015 (O99)	47629.573 (C99)	13.794	0.003	RR _{ab}	1.08 (C99)		15.120	
V115	0.6034 (C99)	47629.772 (C99)	13.639	0.003	RR _{ab}	0.77 (C99)		14.954	no PLK/PLJ-crowded
V116	0.347421 (O99)	47629.518 (C99)	14.071	0.003	RR _c	0.59 (C99)	+0.40	14.787	
V117	0.335578 (O99)	47629.520 (C99)	14.077	0.003	RR _c	0.53 (C99)	-0.48	14.895	
V118	0.5805 (C99)	47629.832 (C99)	13.454	0.004	RR _{ab}	1.57 (C99)	-0.10	14.693	no PLK/PLJ
V119	0.5629 (C99)	47629.297 (C99)	13.783	0.003	RR _{ab}	1.25 (C99)	+0.20	14.935	
V120	0.2797 (C99)	47629.698 (C99)	14.474	0.004	RR _c	0.71 (C99)	+0.10	15.018	no PLK/PLJ-crowded
V121	0.623304 (B96)	47629.303 (C99)	13.733	0.003	RR _{ab}	1.69 (C99)	+0.05	14.846	
V122	0.58048 (Cl)	51946.869*	13.47**		RR _{ab}			14.611	no PLK/PLJ
V123	0.6025 (C99)	47629.303	13.715	0.003	RR _{ab}	0.65 (C99)	-0.10	14.989	
V125	0.3065 (C99)	47629.592 (C99)	13.868	0.005	RR _c	0.65 (C99)		14.933	no PLK/PLJ-crowded
V127	0.544965 (O99)	51946.869*	13.80**		RR _{ab}			15.059	no PLK/PLJ
V128	0.305704 (O99)	47629.785 (C99)	14.240	0.003	RR _c	0.68 (C99)		14.904	
V129	0.6011 (C99)	47629.631 (C99)	13.783	0.003	RR _{ab}	0.74 (C99)		15.112	
V130	0.327396 (R96)	47581.469 (C99)	14.100	0.003	RR _c	0.50 (R96)	+0.46	14.887	
V131	0.281521 (R96)	47629.763 (C99)	14.286	0.003	RR _c	0.68 (C99)	+0.30	15.157	
V132	0.2835 (C99)	47629.648 (C99)	14.255	0.004	RR _c	0.49 (C99)	+0.20	14.974	
V133	0.294905 (Cl99)	52331.804*	14.14**		RR _c			14.869	no PLK/PLJ
V137	0.591 (C99)	47629.520 (C99)	13.825	0.003	RR _{ab}	0.60 (C99)	+0.20	15.020	
V139	0.300 (C99)	47629.587 (C99)	14.186	0.003	RR _c	0.42 (C99)		14.946	
V142	0.4577 (C99)	47629.830 (C99)	14.078	0.003	RR _{ab}	1.5 (C99)		15.194	no PLJ
V155	0.33 (DS)	52331.827*	14.101		RR _c			14.882	no PLK/PLJ
V156	>0.47 (DS)	51946.869*	12.73**		RR _{ab}			14.984	no PLK/PLJ-blended?
V158	0.45 (DS)	51947.004*	13.58**		RR _{ab}			14.235	no PLK/PLJ
V161	0.331570 (O99)	51946.736*	14.035		RR _c			15.051	no PLK/PLJ
V162	0.557468 (O99)	51946.925*	13.86**		RR _{ab}			15.060	no PLK
V163	0.600853 (O99)	52331.773*	13.86**		RR _{ab}			14.912	no PLK

* Epoch of our first measurement.

** Intensity-weighted mean magnitude computed by DAOMASTER.

References:

S91: Storm et al. (1991).

B96: Brocato et al. (1996).

R96: Reid (1996).

DS: Drissen & Shara (1998).

C99: Caputo et al. (1999).

O99: Olech et al. (1999).

K00: Kaluzny et al. (2000).

S10: Szeidl et al. (2010).

bors.

V96: this variable is heavily contaminated by close neighbors.

V104: this variable has been claimed to be a RR_{ab} variable by Reid (1996), but Drissen & Shara (1998) reported it as an eclipsing binary. We found that this variable does not fit the PLK relation (see Fig. 4), since its magnitude is ~ 0.2 mag brighter than the expected magnitude for its period, while the observed dispersion of the PLK relation is ~ 0.15 mag at the 3σ level. This gives support to the Drissen & Shara (1998) interpretation, as also stated in Caputo et al. (1999). However, Olech et al. (1999) reported this star as a multi-periodic variable, with a first overtone radial pulsation and a second period connected with non-radial pulsation.

V106: this variable is heavily contaminated by close neighbors.

V107: this variable is heavily contaminated by close neighbors.

V108 this variable appears to be overluminous in the PLK plane (see Fig. 4), and both overluminous and redder than expected from its pulsation period in the CMD (magenta point in Fig. 2). We therefore suspect that this variable is blended with a red companion, and we excluded it from our analysis.

V111: this variable is heavily contaminated by close neighbors.

V113: according to Caputo et al. (1999) this variable shows a $(B - V)$ color significantly bluer than the blue limit of the instability strip, but with a luminosity which agrees with the average luminosity of the other variables. Excluding subtle effects of blending or crowding, the blue color remains unexplained. However, we found that this variable fairly matches the PLK relation and we used it in our analysis.

V115: this variable is heavily contaminated by close neighbors.

V118: this variable appears to be over-luminous in the PLK plane (green point in Fig. 4), and it has not been used for our PLK analysis. Since it does not seem to be blended, its over-luminosity in the K -band is unexplained. We therefore dropped this star from the present study.

V120: this variable is heavily contaminated by close neighbors.

V125: this variable is heavily contaminated by close neighbors.

V156: this variable appears both overluminous and red in the CMD. We therefore suspected that this variable is blended with a red companion, and we excluded it from our analysis. In Fig. 3 we plot this variable after shifting the K magnitude by 1 mag, to preserve the readability of the figure.

5 THE PLK AND THE PLJ RELATIONS

In the following we compare our data with the available PLK calibrations, which can be divided into three broad groups: pulsational (Bono et al. 2001; Bono et al. 2003), synthetic (Cassisi et al. 2004; Catelan et al. 2004) and empirical (Sollima et al. 2006) PLK relations. We also compare our data with the PLJ calibration provided by Catelan et al. 2004.

Fig. 4 shows the observed mean K -band magnitudes of

the detected variables as a function of the period (observed PLK relation), the empirical fit (rms= 0.05) to the data (blue line) is

$$\langle K \rangle = -2.33(\pm 0.08) \log P + 13.28(\pm 0.02), \quad (1)$$

obtained *fundamentalizing* the first overtone pulsators (filled circles) by applying the relation $\log P_F = 0.127 + \log P_{FO}$ (Di Criscienzo et al. 2004), to use the same PLK relation for fundamental (open circles) and first overtone pulsators. We remark that this offset is consistent with that implied by the difference in $\log P$ at constant $\langle K \rangle$ in Fig. 4. The slope in Eq. 1 is consistent within 1σ with the empirical values found for this cluster (-2.42 ± 0.23 Longmore et al. 1990; -2.27 Sollima et al. 2006, unfortunately without uncertainty). Observed mean K -band magnitudes of RR_{ab} and RR_c are shown separately as a function of the period in Fig. 5. Symbols are the same of Fig. 4. Solid blue and red lines show the empirical fits to the RR_{ab} and RR_c variables, respectively, in particular for the RR_{ab} variables:

$$\langle K \rangle = -2.50(\pm 0.14) \log P + 13.24(\pm 0.04) \quad (2)$$

and for RR_c:

$$\langle K \rangle = -2.66(\pm 0.23) \log P + 12.8(\pm 0.1). \quad (3)$$

By adopting the theoretical calibration of Bono et al. (2001) (their eq. [2]) and a metallicity of $[Fe/H] = -1.26$ (Kraft & Ivans 2003), we can determine the individual distance moduli of the RRLs. The observations were transformed into the Bessell & Brett (1988) homogenized Johnson-Cousins-Glass photometric system according to the relation $K_{BB} = K_{2M} + 0.044$ mag provided by Carpenter (2001). The weighted average of these estimates gives an apparent distance modulus $DM_K = (14.42 \pm 0.06)$ mag, where the adopted uncertainty is the standard deviation (rms). The adopted reddening toward M5 is $E(B - V) = 0.03$ mag, as taken from the Harris (2010) catalog. We combine this value with the reddening law from Cardelli et al. (1989) of $A_K = 0.114 \times 3.1 \times E(B - V)$ which gives an absorption in the K -band of $A_K = 0.011$ mag. Correcting the distance modulus for the reddening, we find that the true value is $DM_0 = (14.41 \pm 0.06)$ mag. These results indicate that the current distance estimate to M5 is minimally affected by reddening uncertainties and by uncertainties in the extinction law (McCall 2004; Bono et al. 2010).

In order to improve the theoretical calibration of the PLZ_K relation, Bono et al. (2003) devised a new pulsation approach that relies on mean K -band magnitudes and $(V - K)$ colors. In particular, they derived new period-luminosity-color-metallicity relations for RR_{ab} and RR_c variables (see their relations [7] and [8]) that include the luminosity term. According to these relations, one finds that accurate V , K photometric measurements of both RR_{ab} and RR_c variables provide excellent proxies for the effective temperature, and can in turn be adopted to estimate the luminosity level. We therefore adopted accurate V -band magnitudes extracted by optical light curves of the PBS unpublished archive (shown in the last column of Table 2) and we compared our empirical slopes in Eqs. 2 and 3 with the theoretical predictions, being -2.102 and -2.265 for RR_{ab} and RR_c stars, respectively. Once we transform the observations into the Bessell & Brett (1988) system and after correcting for the reddening, we find a value of $DM_0 = (14.46 \pm 0.09)$ rms mag

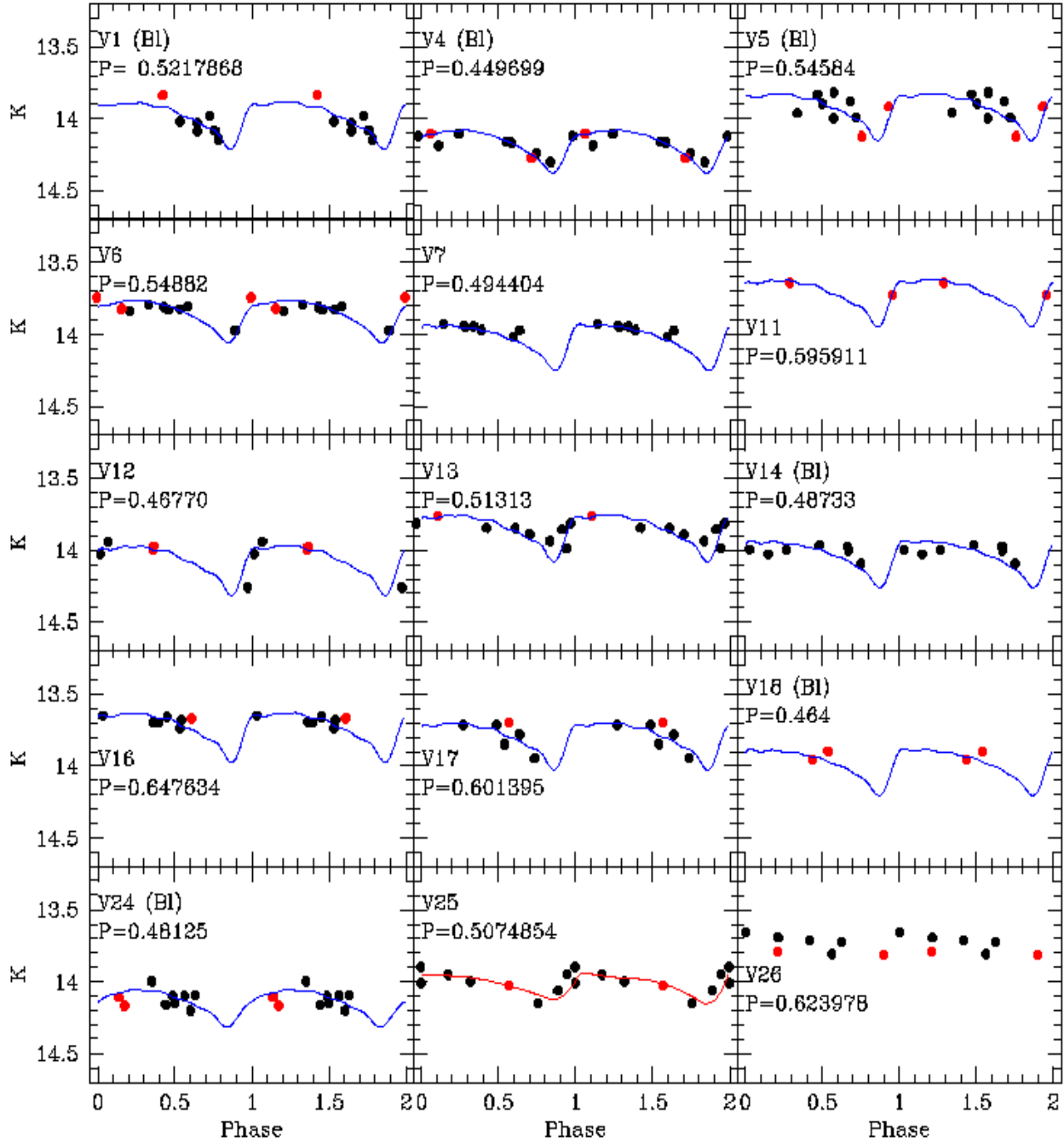
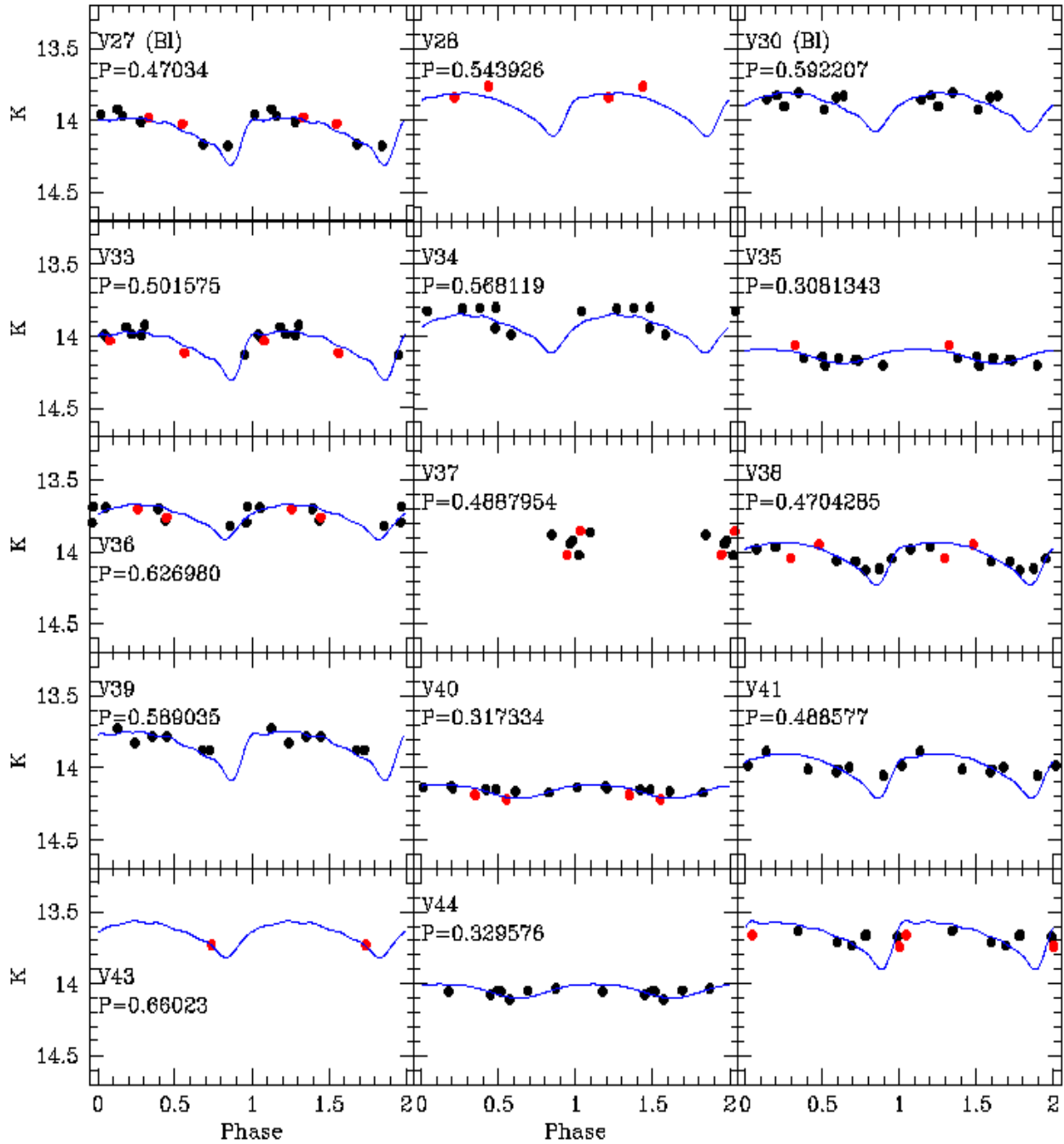


Figure 3. K -band light curves for all RRLs in our fields. Black and red points mark SOFI and NICS data, respectively. The blue solid lines show, when available, the fit with the template light curve, while the red line the fit with a spline.

using the RR_{ab} stars, while using the RR_c stars we find $DM_0 = (14.46 \pm 0.05 \text{ rms})$ mag. Note that the dispersion of the distance estimates based on RR_c stars is almost a factor of two smaller than the distance based on RR_{ab} stars, because the width in temperature of the region of the instability strip in which the FOs are pulsationally stable is typ-

ically a factor of two narrower than for the Fs. This means that the intrinsic dispersion in the infrared luminosity of FOs is systematically smaller than for Fs.

The evolutionary calibrations by Cassisi et al. (2004) and Catelan et al. (2004) are based on the Horizontal Branch morphology and on the RRL pulsational proper-

Figure 3 – *continued*

ties. These authors provide period-luminosity relations in the Johnson-Cousins-Glass photometric system, with slopes and zero-points that vary with the HB morphology and with the metallicity. In particular, Cassisi et al. (2004) gives a grid of slopes and zero-points as a function of the metallicity (expressed as the mass fraction Z) and the HB type

(HBT, according to the Lee, Demarque & Zinn parameter, Lee et al. 1994). We chose, among the values available in their published grid, $Z = 0.0006$ and $HBT = 0.28$ since these parameters are those closest to the M5 literature values ($HBT = 0.31$, taken from the Harris 2010 catalog), obtaining the calibration $M_K = -2.34(\log P_F + 0.30) - 0.394$. Once

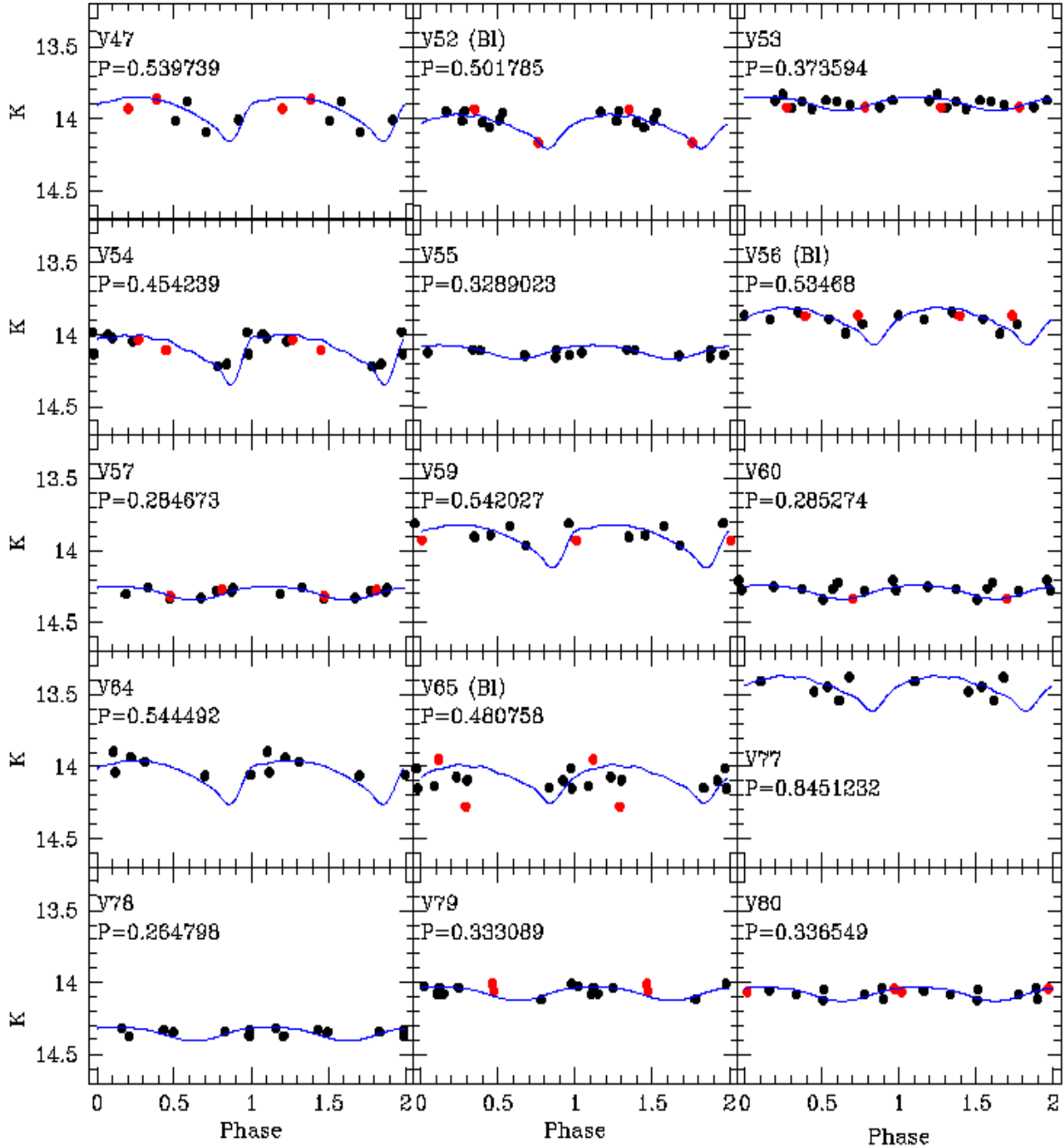
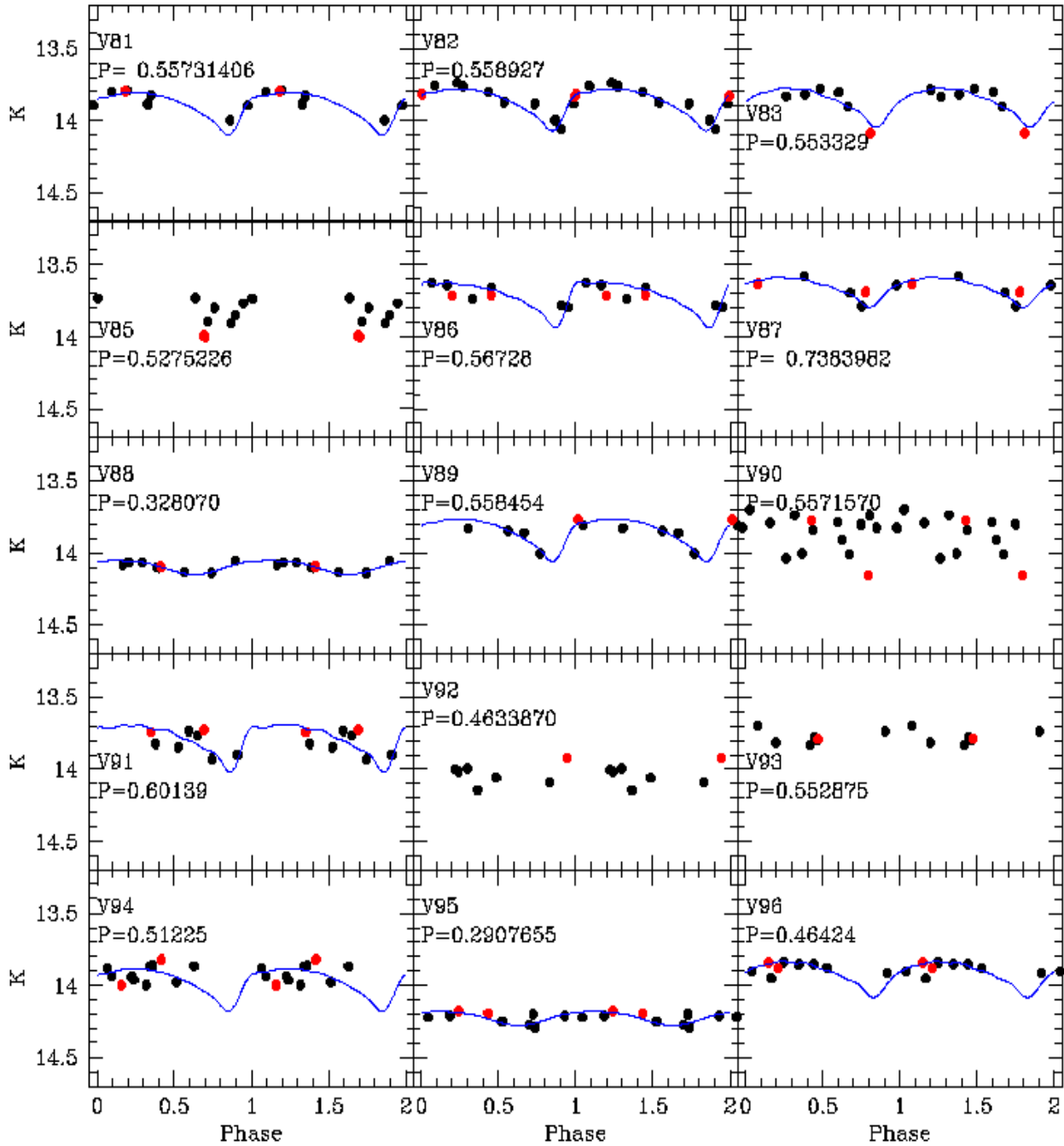


Figure 3 – continued

we apply the correction for the difference in the photometric system and for the reddening, and having fundamentalized RR_c variables, we find a true distance modulus to M5 of $DM_0 = (14.41 \pm 0.05 \text{ rms}) \text{ mag}$.

A very similar approach was devised by Catelan et al. (2004) who provided *average* relations, to be used when the

HB type is not known *a priori*. However, we adopted their calibration with $Z = 0.0005$ and $HBT = 0.414$, obtaining the calibration $M_K = -2.355(\log P_F) - 1.172$. Again, once we apply the correction for the difference in the photometric system and for the reddening, and having fundamentalized

Figure 3 – *continued*

the RR_c variables, we found a true distance modulus to M5 of $DM_0 = (14.48 \pm 0.05 \text{ rms}) \text{ mag}$.

Finally, we also adopted the empirical calibration by Sollima et al. (2006) ($M_K = -2.38 \log P_F + 0.09 [\text{Fe}/\text{H}] - 1.04$) and we found a true distance modulus of $DM_0 = (14.41 \pm 0.05 \text{ rms}) \text{ mag}$. It is interesting to note

that Sollima et al. (2006), using a collection of data for 86 RRLs, found a true distance to M5 ($14.35 \pm 0.15 \text{ mag}$) that agrees well with the current estimates.

We end this section with a discussion of the observed PLJ relation. Fig. 6 shows observed mean J magnitudes of the considered RRLs vs. $\log P$. The RR_c variables have

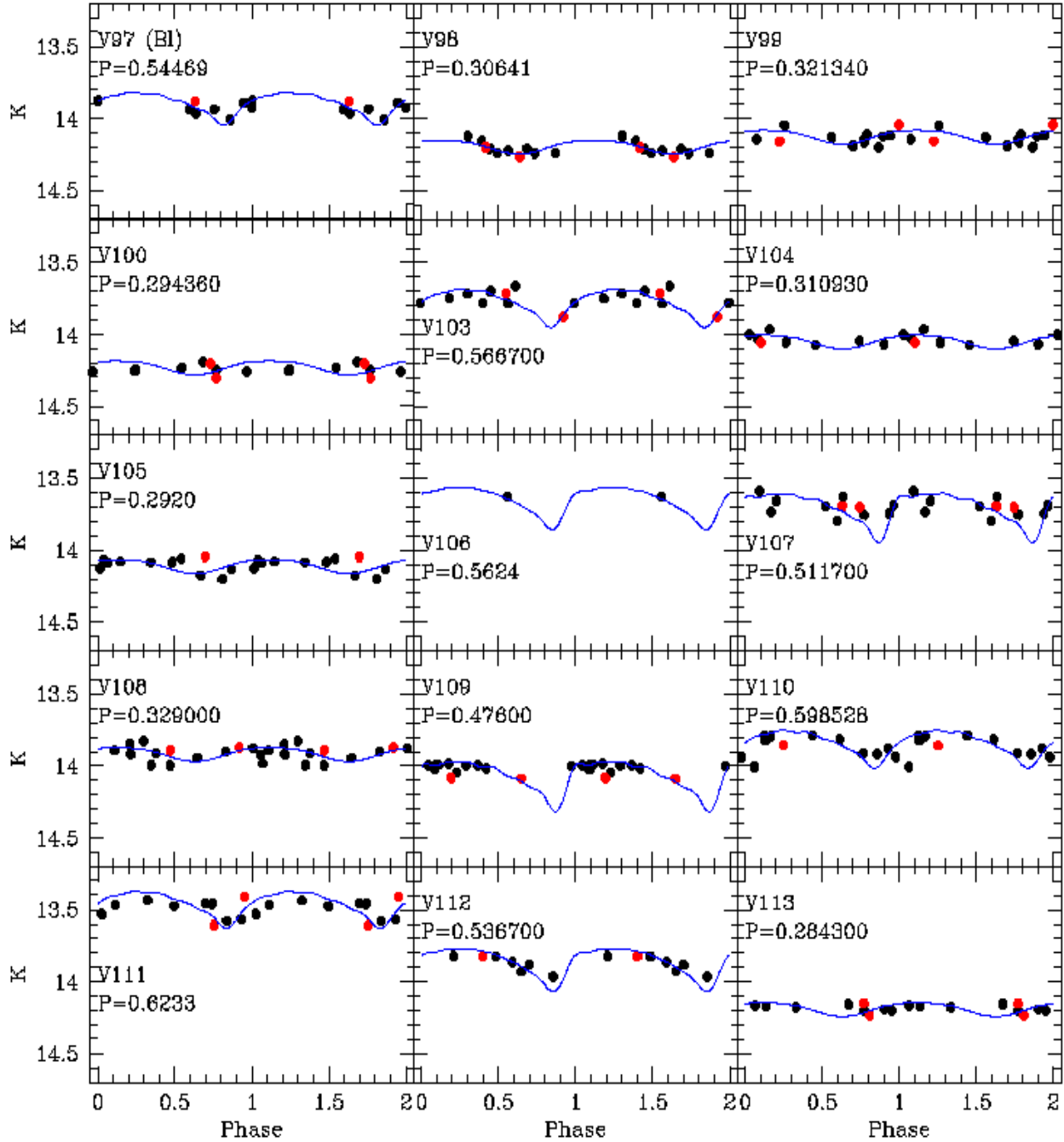
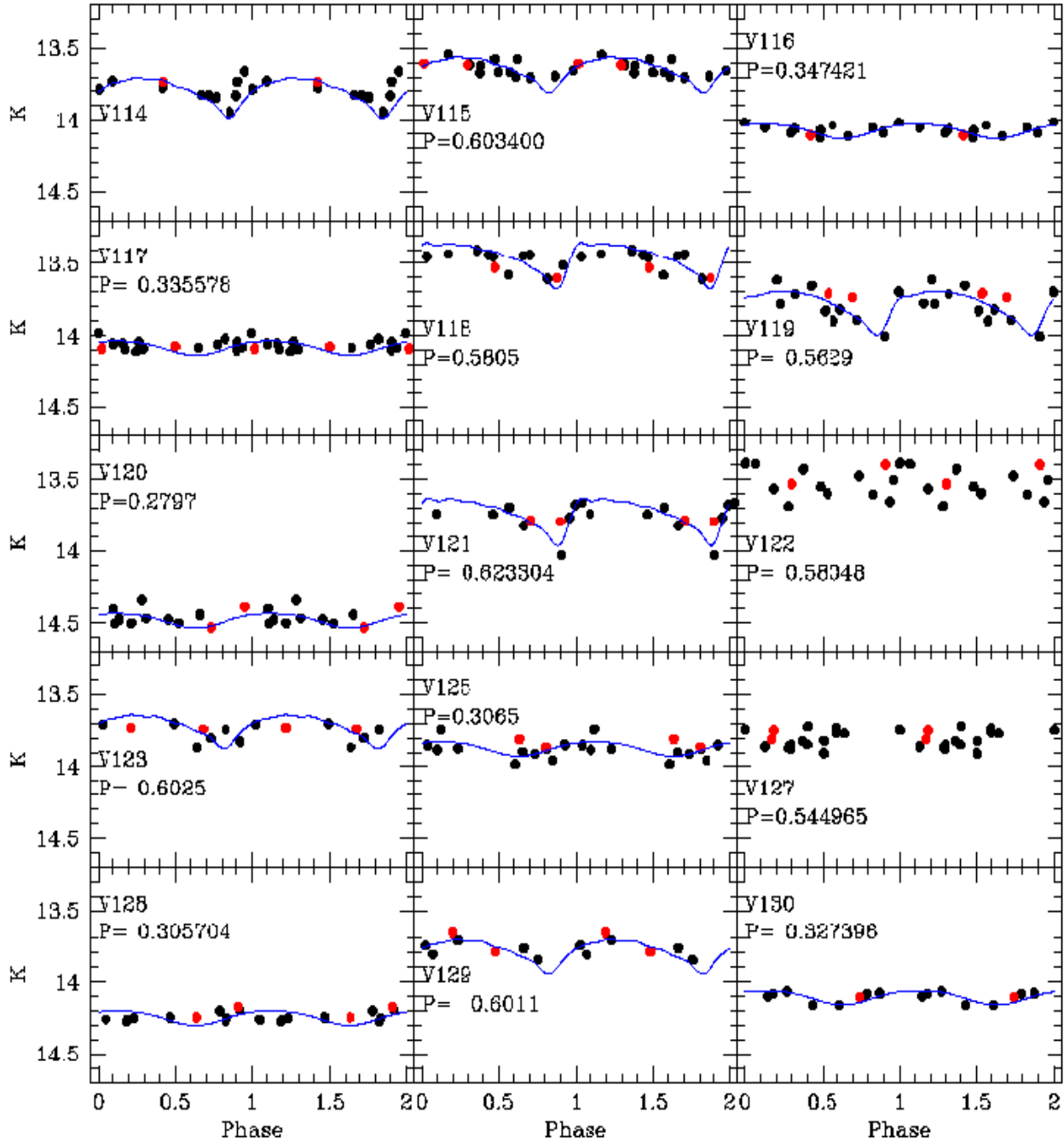


Figure 3 – continued

been fundamentalized. Since in the literature there are no suitable templates to adopt, and since the uneven phase coverage of the observations did not allow us to interpolate the observed data with spline curves, we simply used intensity-weighted mean magnitudes, as computed with DAOMASTER. To reduce subtle effects for uneven light curve sam-

pling, we used for the PLJ only stars with a good phase coverage, therefore ending up with 35 RR_{ab} and 23 RR_c stars. The observed slope is -1.85 ± 0.14 , which is in very good agreement with the available theoretical calibration ($M_J = -1.773 \log P + 0.190 \log Z - 0.141$, Catelan et al. 2004). In passing, we note that F and FO pulsators seem

Figure 3 – *continued*

to not follow a common relation even after fundamentalization, with the F variables alone apparently following a steeper distribution. On the other hand, we point out that the Catelan et al. 2004 calibration used as reference is obtained by using both RR_{ab} and RR_c stars. We transformed the observations in the Bessell & Brett

(1988) homogenized Johnson-Cousins-Glass J system with the relation $J_{BB} = J_{2M} - 0.029(J - K)_{2M} + 0.053$, derived following the Carpenter (2001) equations. After correcting for the extinction with the Cardelli et al. (1989) law, we get a true PLJ-based distance to M5 of (14.50 ± 0.08) mag, in agreement with the PLK calibrations. We explicitly note

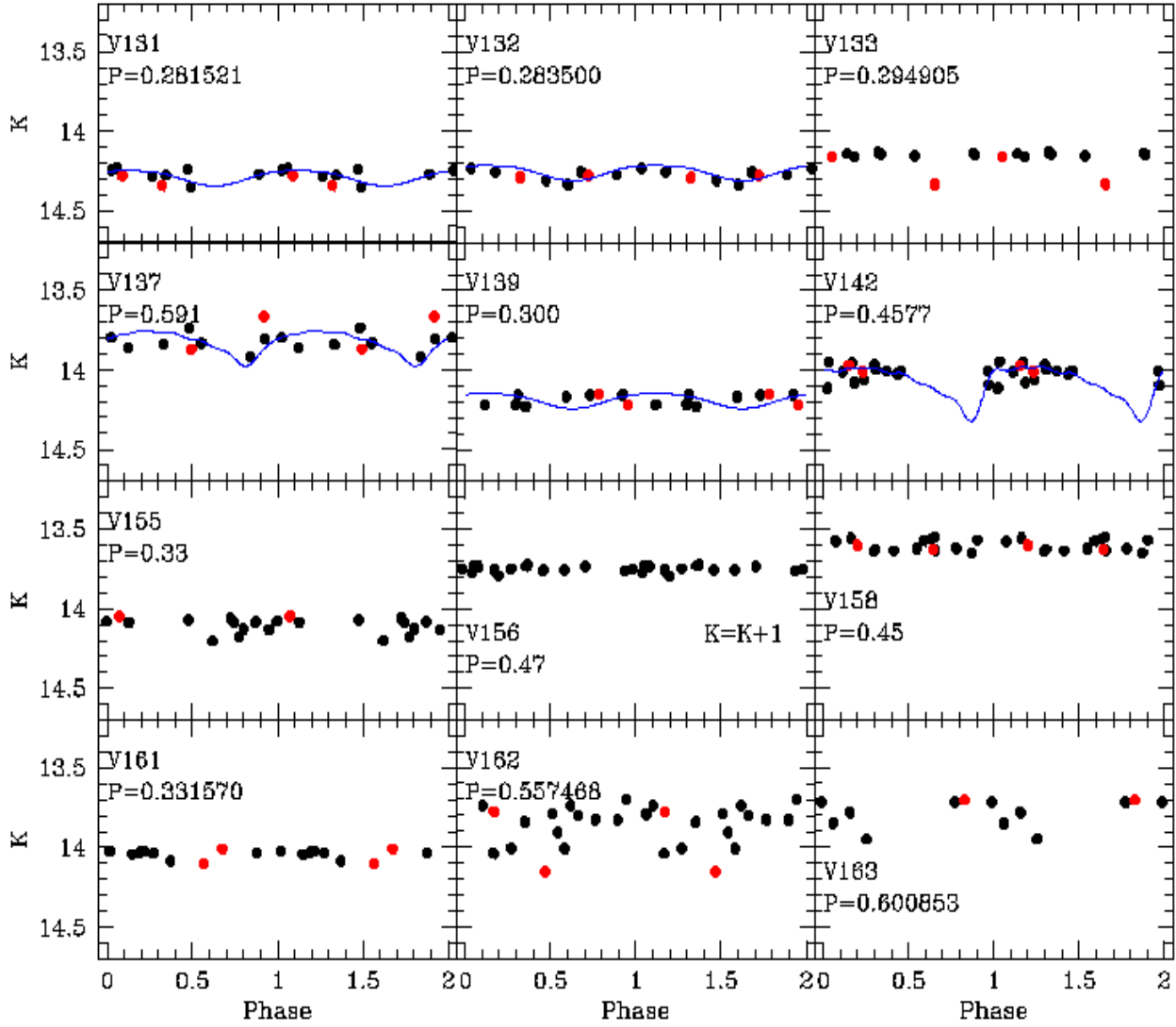


Figure 3 – continued The K-band magnitudes of V156 have been artificially shifted by 1 mag to make more clear the figure.

that the distances based on the two PLK and PLJ calibrations provided by Catelan et al. (2004) are slightly longer than the others, but with an excellent internal agreement.

All predicted and empirical slopes and the distance moduli based on the above relations are listed in Table 3.

6 DISCUSSION

On the basis of our data, we found that the weighted mean of the different theoretical and empirical calibrations of the PLK relation gives a true distance modulus of 14.44 ± 0.02 mag.

The distance to M5 based on the PLK relation also

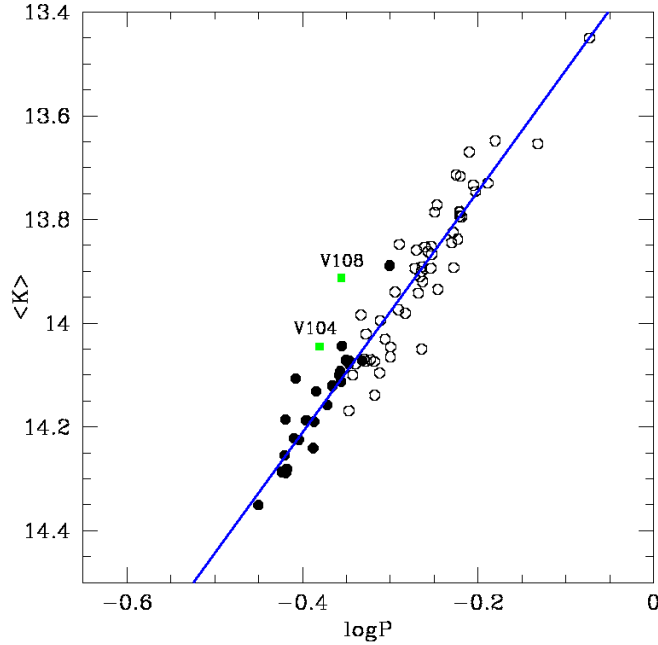


Figure 4. Empirical $\log P - \langle K \rangle$ relation of the M5 RRLs. Filled circles show the fundamentalized RR_c stars. Open circles are RR_{ab} stars, and the solid blue line represents the empirical fit to the data.

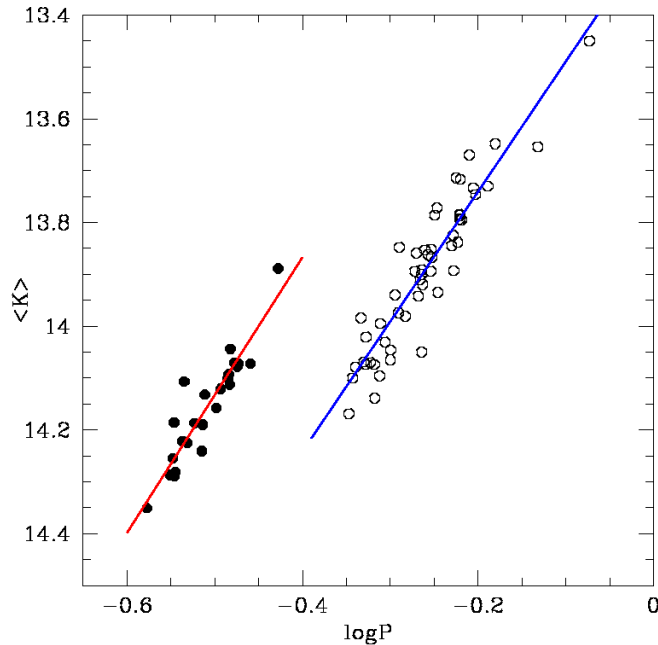


Figure 5. Observed $\log P - \langle K \rangle$ relation of the M5 RRLs. Filled circles show the RR_c stars, while open circles are RR_{ab} stars. Solid blue and red lines represent the empirical fit to the data.

agrees quite well with similar estimates available in the literature, but based on different distance indicators. The distance estimates listed in Table 4 indicate quite clearly that the current distance agrees within 1σ with distance based not only on the PLK relation (14.35 ± 0.15 mag Sollima et al. 2006), but also on main-sequence fitting method (Reid 1998; Carretta et al. 2000; Layden et al. 2005) and semi-geometric

approach (14.37 ± 0.18 mag Storm et al. 1994). On the other hand, our distance is systematically longer than the distance to M5 provided by Di Criscienzo et al. (2004) using synthetic horizontal branch models and pulsation properties of RRLs and the difference is larger than 1σ .

In this context it is noteworthy that the distance based on the PLK relation agrees with the distance based on the

Table 3. NIR PL slope and true distance moduli for different adopted calibrations. F and FO labels refer to fundamental and first overtone variables, respectively. The adopted error is the rms of the distribution of the estimates on individual RRLs.

Calibration	Predicted slope	Sample	Our Empirical J slope	Our Empirical K slope	DM_0 (mag)
Bono et al. (2001)	-2.031	F + FO	—	-2.33 ± 0.08	14.41 ± 0.06
Bono et al. (2003)	-2.102	F	—	-2.50 ± 0.14	14.46 ± 0.09
Bono et al. (2003)	-2.265	FO	—	-2.66 ± 0.23	14.46 ± 0.05
Cassisi et al. (2004)	-2.34	F+FO	—	-2.33 ± 0.08	14.41 ± 0.05
Catelan et al. (2004)	-2.355	F+FO	—	-2.33 ± 0.08	14.48 ± 0.05
Catelan et al. (2004)	-1.773	F+FO	-1.85 ± 0.14	—	14.50 ± 0.08
Sollima et al. (2006)	-2.38	F+FO	—	-2.33 ± 0.08	14.41 ± 0.05

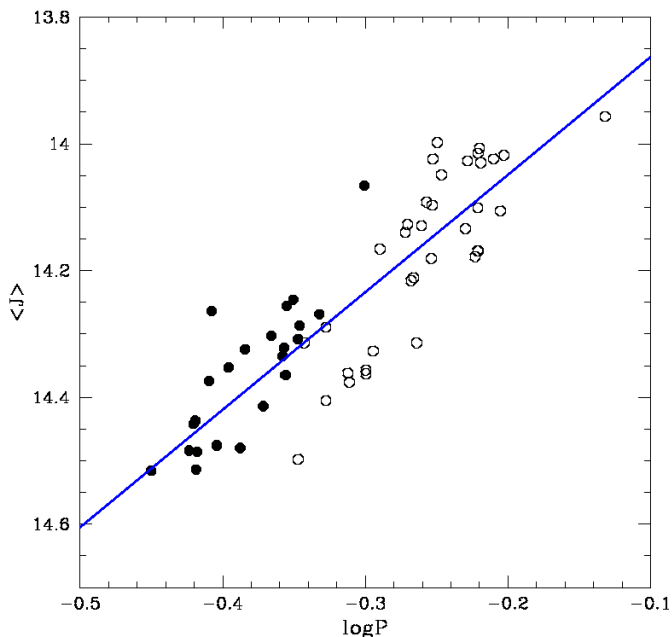


Figure 6. Observed $\log P - \langle J \rangle$ relation of the M5 RRLs. Filled circles show fundamentalized RR_c stars, while open circles are RR_{ab} stars. Solid blue line represents the empirical fit to the data.

proper motions $(m - M)_0 = 14.44 \pm 0.41$ mag by Rees (1996). Even though the intrinsic error of the quoted distance estimates differ by more than one order of magnitude, the two distances taken at face value agree quite well. If this agreement is not fortuitous, due to the large error bar in the Rees (1996) estimate, this would be first time that kinematic distances agree with other distance indicators. Typically, the kinematic distances to GCs are 0.2-0.3 magnitudes smaller than distance moduli based either on the PLK relation of RRLs, or on main-sequence fitting, or on the tip of the Red Giant Branch (TRGB, Bono et al. 2008). The reasons for such discrepancies are not clear yet, but the current agreement appears very promising to further constrain the occurrence of possible systematic errors.

On the other hand, the distance based on the fitting of the White dwarf cooling sequence $(m - M)_0 = 14.67 \pm 0.18$ mag provided by Layden et al. (2005) is approximately 0.2 mag larger than distances based on other methods. The difference with the distance based on the PLK relation and on main-sequence fitting is on average slightly larger than 1σ . This is also an interesting occurrence, since distance mod-

uli to GCs based on the fitting of the white-dwarf cooling sequence are typically 0.1-0.3 mag smaller than distances to GCs based either on the TRGB, or on the PLK relation or on the main sequence fitting (Bono et al. 2008; Moehler & Bono 2008).

We have also investigated the PLJ relation of RRL stars in M5, and from a sample of 35 RRab and 23 RRc (fundamentalized) variables we found an empirical slope of -1.85 ± 0.14 . The uncertainty in the slope of the PLJ relation is almost a factor of two larger than the uncertainty in the slope of the PLK relation (0.14 vs 0.08) because the luminosity amplitude in the J -band is larger in the K -band, and also because we still lack accurate J -band light curve templates. Therefore, the mean J -band magnitudes were estimated as a time average and only for RRLs with good phase coverage. Homogeneous sets of time series data both in J and K are required to constrain on an empirical basis the intrinsic spread of PLK and PLJ relations. Finally, we mention that by adopting the calibration of the PLJ relation provided by Catelan et al. (2004), we found a true distance modulus to M5 of 14.50 ± 0.08 mag. The distances based on

Table 4. Summary of some of the M5 distance estimates available in the literature.

Study	Method	[Fe/H]	Reddening	DM ₀ (mag)
Sollima et al. (2006)	PLK	-1.10	$E(B - V) = 0.035$	14.35 ± 0.15
Reid (1998)	Main sequence fitting	-1.10	$E(B - V) = 0.02$	14.52 ± 0.15
Carretta et al. (2000)	Main sequence fitting	-1.10	$E(B - V) = 0.035$	14.48 ± 0.05
Layden et al. (2005)	Main sequence fitting	-1.11	$E(V - I) = 0.046$	14.45 ± 0.11
Storm et al. (1994)	Baade-Wesselink	-1.40	$E(V - I) = 0.02$	14.37 ± 0.18
Di Criscienzo et al. (2004)	RRL pulsation properties	-1.26	$E(B - V) = 0.03$	14.32 ± 0.04
Rees (1996)	Proper motions	14.44 ± 0.41
Layden et al. (2005)	White dwarf fitting	-1.11	$E(V - I) = 0.046$	14.67 ± 0.18

the PLJ and on the PLK relations agree quite well, but the intrinsic error of the former is a factor of two larger.

The distances to M5 based either on the PLK or on the PLJ relation agree quite well with distances based on independent robust standard candles. This finding further supports the key role that accurate NIR photometry of cluster variables (RRL, type II Cepheids) can play in the improvement of GC distance scale (Matsunaga et al. 2010). Moreover and even more importantly, the comparison with M5 distances based on different distance indicators strongly supports the evidence that M5 might be a fundamental laboratory to constrain on a quantitative basis the thorny systematic uncertainties that might affect the most popular primary distance indicators. It goes without saying that this sanity check would benefit by further improvements in the precision of the kinematic distances and/or in the geometrical distances based on possible eclipsing binary systems in M5.

In a future paper we plan to compare optical and NIR photometry of M5 with evolutionary predictions, in particular for advanced evolutionary phases.

ACKNOWLEDGMENTS

We sincerely thank an anonymous referee for her/his helpful comments, which improved the readability of the paper.

GC is supported by the Italian Ministry of Education, University and Research (MIUR) grant PRIN-MIUR 2007:*Multiple stellar populations in globular clusters: census, characterization and origin* P.I.: G. Piotto.

This research has made use of the SIMBAD data base, operated at CDS, Strasbourg, France. This publication makes use of data products from the Two Micron All Sky Survey, which is a joint project of the University of Massachusetts and the Infrared Processing and Analysis Center/California Institute of Technology, funded by the National Aeronautics and Space Administration and the National Science Foundation.

REFERENCES

Bailey, S. I., & Pickering, E. C. 1917, *Annals of Harvard College Observatory*, 78, 99
 Bessell, M. S., & Brett, J. M. 1988, *PASP*, 100, 1134
 Bica, E., Bonatto, C., Barbuy, B., & Ortolani, S. 2006, *A&A*, 450, 105

Bono, G., Caputo, F., Castellani, V., Marconi, M., & Storm, J. 2001, *MNRAS*, 326, 1183
 Bono, G. 2003, *Stellar Candles for the Extragalactic Distance Scale*, 635, 85
 Bono, G., Caputo, F., Castellani, V., Marconi, M., Storm, J., & Degl'Innocenti, S. 2003, *MNRAS*, 344, 1097
 Bono, G., et al. 2008, *ApJL*, 686, L87
 Bono, G., et al. 2010, *ApJL*, 708, L74
 Brocato, E., Castellani, V., & Ripepi, V. 1996, *AJ*, 111, 809 (B96)
 Butler, D. 1975, *ApJ*, 200, 68
 Cacciari, C., & Clementini, G. 2003, *Stellar Candles for the Extragalactic Distance Scale*, 635, 105
 Caputo, F., Castellani, V., Marconi, M., & Ripepi, V. 1999, *MNRAS*, 306, 815 (C99)
 Cardelli, J. A., Clayton, G. C., & Mathis, J. S. 1989, *ApJ*, 345, 245
 Carpenter, J. M. 2001, *AJ*, 121, 2851
 Carretta, E., Gratton, R. G., Clementini, G., & Fusi Pecci, F. 2000, *ApJ*, 533, 215
 Carretta, E., Bragaglia, A., Gratton, R., D'Orazi, V., & Lucatello, S. 2009, *A&A*, 508, 695
 Cassisi, S., Castellani, M., Caputo, F., & Castellani, V. 2004, *A&A*, 426, 641
 Cassisi, S. 2010, *IAU Symposium*, 262, 13
 Catelan, M., Pritzl, B. J., & Smith, H. A. 2004, *ApJS*, 154, 633
 Clement, C. M., et al. 2001, *AJ*, 122, 2587 (Cl)
 Cohen, J. G., & Matthews, K. 1992, *PASP*, 104, 1205
 Cudworth, K. M., & Hanson, R. B. 1993, *AJ*, 105, 168
 Dall'Ora, M., et al. 2003, *AJ*, 126, 197
 Dall'Ora, M., et al. 2004, *ApJ*, 610, 269
 Dall'Ora, M., et al. 2006, *ApJL*, 653, L109
 Del Principe, M., Piersimoni, A. M., Bono, G., Di Paola, A., Dolci, M., & Marconi, M. 2005, *AJ*, 129, 2714
 Del Principe, M., et al. 2006, *ApJ*, 652, 362
 Di Criscienzo, M., Marconi, M., & Caputo, F. 2004, *ApJ*, 612, 1092
 Drissen, L., & Shara, M. M. 1998, *AJ*, 115, 725 (DS)
 Evstigneeva, N. M., Shokin, Y. A., Samus, N. N., & Tsvetkova, T. M. 1999, *VizieR Online Data Catalog*, 902, 10509
 Feast, M. W., Laney, C. D., Kinman, T. D., van Leeuwen, F., & Whitelock, P. A. 2008, *MNRAS*, 386, 2115
 Fiorentino, G., et al. 2010, *ApJ*, 708, 817
 Forbes, D. A., & Bridges, T. 2010, *MNRAS*, 404, 1203
 Frogel, J. A., Persson, S. E., Matthews, K., & Aaronson, M. 1978, *ApJ*, 220, 75
 Gerashchenko, A. 1987, *Information Bulletin on Variable*

- Stars, 3044, 1
- Gratton, R. G., Fusi Pecci, F., Carretta, E., Clementini, G., Corsi, C. E., & Lattanzi, M. 1997, *ApJ*, 491, 749
- Greco, C., et al. 2009, *ApJ*, 701, 1323
- Harris, W. E. 1996, *AJ*, 112, 1487
- Harris, W. E. 2010, arXiv:1012.3224
- Jurcsik, J., et al. 2010, arXiv:1010.1119 (J10)
- Jones, R. V., Carney, B. W., & Fulbright, J. P. 1996, *PASP*, 108, 877
- Kaluzny, J., Olech, A., Thompson, I., Pych, W., Krzeminski, W., & Schwarzenberg-Czerny, A. 2000, *A&AS*, 143, 215 (K00)
- Kraft, R. P., & Ivans, I. I. 2003, *PASP*, 115, 143
- Kravtsov, V. V. 1988, *Astronomicheskij Tsirkulyar*, 1526, 6
- Layden, A. C., Sarajedini, A., von Hippel, T., & Cool, A. M. 2005, *ApJ*, 632, 266
- Law, D. R., & Majewski, S. R. 2010, *ApJ*, 718, 1128
- Lee, Y.-W., Demarque, P., & Zinn, R. 1994, *ApJ*, 423, 248
- Longmore, A. J., Fernley, J. A., & Jameson, R. F. 1986, *MNRAS*, 220, 279
- Longmore, A. J., Dixon, R., Skillen, I., Jameson, R. F., & Fernley, J. A. 1990, *MNRAS*, 247, 684
- Mackey, A. D., & van den Bergh, S. 2005, *MNRAS*, 360, 631
- Marconi, M., Caputo, F., Di Criscienzo, M., & Castellani, M. 2003, *ApJ*, 596, 299
- Matsunaga, N., et al. 2006, *MNRAS*, 370, 1979
- Matsunaga, N., Feast, M. W., & Soszynski, I. 2010, arXiv:1012.0098
- McCall, M. L. 2004, *AJ*, 128, 2144
- Meylan, G., & Heggie, D. C. 1997, *A&AR*, 8, 1
- Moehler, S., & Bono, G. 2008, arXiv:0806.4456
- Olech, A., Woźniak, P. R., Alard, C., Kaluzny, J., & Thompson, I. B. 1999, *MNRAS*, 310, 759 (O99)
- Oosterhoff, P. T. 1939, *The Observatory*, 62, 104
- Oosterhoff, P. T. 1941, *Annalen van de Sterrewacht te Leiden*, 17, 1 (O41)
- Pietrzyński, G., & Gieren, W. 2002, *AJ*, 124, 2633
- Pietrzyński, G., et al. 2008, *AJ*, 135, 1993
- Rees, R. F., Jr. 1996, *Formation of the Galactic Halo...Inside and Out*, 92, 289
- Reid, N. 1996, *MNRAS*, 278, 367 (R96)
- Reid, I. N. 1997, *AJ*, 114, 161
- Reid, N. 1998, *AJ*, 115, 204
- Renzini, A., & Fusi Pecci, F. 1988, *AR&A*, 26, 199
- Samus, N. N., Kazarovets, E. V., Pastukhova, E. N., Tsvetkova, T. M., & Durlevich, O. V. 2010, *VizieR Online Data Catalog*, 612, 11378
- Sandquist, E. L., Bolte, M., Stetson, P. B., & Hesser, J. E. 1996, *ApJ*, 470, 910
- Sawyer Hogg, H. 1973, *Publications of the David Dunlap Observatory*, 3, 6
- Sollima, A., Cacciari, C., & Valenti, E. 2006, *MNRAS*, 372, 1675
- Stetson, P. B. 1987, *PASP*, 99, 191
- Stetson, P. B. 1994, *PASP*, 106, 250
- Stetson, P. B., Bruntt, H., & Grundahl, F. 2003, *PASP*, 115, 413
- Storm, J., Carney, B. W., & Beck, J. A. 1991, *PASP*, 103, 1264 (S91)
- Storm, J., Carney, B. W., & Latham, D. W. 1994, *A&A*, 290, 443
- Skrutskie, M. F., et al. 2006, *AJ*, 131, 1163
- Szeidl, B., et al. 2010, arXiv:1010.1115 (S10)
- Yang, S.-C., Sarajedini, A., Holtzman, J. A., & Garnett, D. R. 2010, *ApJ*, 724, 799
- Wainscoat, R. J., & Cowie, L. L. 1992, *AJ*, 103, 332
- Zinn, R. 1985, *ApJ*, 293, 424